

Road Graph Generator: Mapping roads at construction sites from GPS data

Katarzyna Michałowska, Helga Margrete Bodahl Holmestad, Signe Riemer-Sørensen

Mathematics and Cybernetics, SINTEF Digital, Oslo, Norway

Abstract

We propose a new method for inferring roads from GPS trajectories to map construction sites. This task presents a unique challenge due to the erratic and non-standard movement patterns of construction machinery, which significantly diverge from typical vehicular traffic on established roads. Our proposed method first identifies intersections in the road network that serve as critical decision points, and then connects them with edges to produce a graph, which can subsequently be used for planning and task-allocation. We demonstrate the approach by mapping roads at a real-life construction site in Norway. The method is validated on four increasingly complex segments of the map. In our tests, the method achieved perfect accuracy in detecting intersections and inferring roads in data with no or low noise, while its performance was reduced in map areas with significant noise and consistently missing GPS updates.

Keywords: Road inference, GPS trajectory, spatial graph detection from GPS data, trajectory alignment

1. Motivation

Reducing carbon emissions is a critical goal in mitigating the far-reaching impacts of climate change. In Norway, the building and construction sector contributes directly and indirectly to 15% of total greenhouse gas emissions (2019), with construction vehicles accounting for 1.5% of the total emissions (2021) [1, 2].

In managing construction projects, it is crucial to effectively handle the complex interplay of resources, including personnel, materials, and machin-

ery, to ensure their optimal interaction in terms of type, quantity, location, and timing [3]. One viable strategy to address this issue is to maximize the utilization of heavy machinery, such as dump trucks and excavators, through optimal coordination and task allocation. According to Skanska Norge AS, the largest construction contractor in Norway, mass transporting units are idling 40–60% of the time during projects. This is a consequence of the conventional planning approach where excavators are considered more expensive than mass transportation units, and hence the latter are excessively deployed to avoid idling excavators, often leading to over-capacity and idling of transportation units instead. Improved coordination on construction sites, e.g., optimized real-time task allocation for dumpers, can reduce this over-capacity, leading to lower greenhouse gas emissions and saving both time and money. This is a critical improvement given the increasing size of construction projects involving hundreds of mass transporting units.

The first step in optimizing these operations is acquiring an up-to-date map of the construction site. It is imperative that the map generation be automated given the constantly evolving nature of the construction site, and because manual mapping would be impractical and deprioritized, as emphasized in interviews with drivers, foremen and construction site coordinators. Herein, we address this need by proposing an algorithm for road inference from Global Positioning System (GPS) trajectories recorded by vehicles on the construction site. Our algorithm generates a graph consisting of road intersections (nodes) and road centerlines (edges), which is a formulation that conveniently allows for the subsequent use of standard resource planning and optimization techniques. Furthermore, utilizing movement data, as opposed to e.g., aerial images facilitates identification of temporary roads which are typically less visible or distinguishable in the terrain and does not require frequent collection of aerial images to capture the dynamic changes.

2. Related work

Automated road inference plays a pivotal role in various applications, such as urban planning, transportation management, and autonomous driving. The primary machine learning approaches for map generation are either from images, e.g., aerial photos, drone-, or satellite imagery [4, 5, 6, 7, 8], or from movement data, such as GPS trajectories [9, 10, 11]. The latter approach becomes particularly advantageous when paths are not easily distinguishable in images, e.g., blend into the surrounding environment. Moreover, GPS data

collection is cost-effective compared to aerial or satellite imagery, especially for repeated acquisitions over time, since it can leverage existing devices like mobile phones.

In the context of optimizing vehicle operations at construction sites, it is advantageous to model the road network as a graph. In such model, intersections are treated as key decision points, represented as nodes, while the roads themselves are depicted as the connecting edges between these nodes. Moreover, graph representation is more compact compared to alternatives like raster images. We therefore direct our attention to works that detect road intersections and infer road centerlines, i.e., central paths along the roads.

In CellNet [9], the approach involves dividing the map into a grid and applying the mean-shifting algorithm on all GPS points within each cell, which results in identifying intersections, if they are present within the cell, or pinpointing the center of the stream of routes otherwise. To filter out the latter, each potential intersection is verified to have at least three outgoing streams of routes by clustering the points within a predefined annulus around the candidate. The clustering approach is shown in Figure 2 as we adapt the filtering and clustering approaches to our purpose as described in section 6. In CellNet, the roads connecting the identified intersections are modeled using FastDTW, a fast and approximate implementation of dynamic time warping (DTW).

Another approach to detect intersections involves initially identifying turning points by analyzing the difference in heading directions during individual trips, followed by clustering these turning points based on Euclidean distance [10]. To reduce the incidence of falsely identified intersections, only clusters with multiple points are retained. Additionally, the heading directions into and out of each potential intersection are compared with each other to remove road bends. Similarly to CellNet, the tracks connecting the intersections are aligned using dynamic time warping.

In COLTRANE (ConvolutiOnaL TRAjectory NEtwork) [11], the authors propose a variation of the mean-shifting algorithm termed iterated trajectory mean shift (ITMS) to identify road centerlines. The road centerlines are treated as nodes, and the candidate edges are inferred based on the distance of the GPS points from the centerlines. Finally, the edges are classified and pruned with a convolutional neural network with custom input features derived from 2D histograms of location and directional velocities.

The aforementioned methods have demonstrated strong performance in

structured environments, such as cityscapes [9, 10, 11] and airport tarmacs [11]. However, the movement patterns of vehicles at construction sites differ from these environments, and include reversing and maneuvering into specific positions for loading and unloading of the materials, navigating through narrow roads and rugged terrain, wide open areas, variable speeds and frequently stopping and starting. To address these unique challenges, we propose a multi-step method that first identifies the intersections in the road network and subsequently connects the roads, thereby bridging the gap in current methodologies for construction site applications.

3. Problem definition

The objective is to use GPS data to infer a graph representing the underlying road network, where each node of the graph represents a road intersection or an action point (loading or off-loading) which is described as a vector of latitude, longitude and altitude $I = (lat, lon, altitude)$. An intersection is defined as a point where at least three roads meet. The edges of the graph represent the roads and are defined as a series of consecutive, equidistant points $E = (lat, lon, altitude)$. An example of a graph is shown in Fig. 3.

4. Data description

The data used for demonstration consists of GPS updates of a fleet of dumper trucks operating at the E18 Bjørrum-Skaret construction site in Norway over one day (5:00 a.m. UTC, September 13–14, 2022). The information is organized as time series and segmented into 612 distinct trips, where each trip begins when the truck is being loaded by an excavator and ends when a new one starts, therefore each trip includes phases of truck loading, driving, material delivery, and traveling empty to the next loading location. Every individual position update is defined by a timestamp, geographical coordinates (lat, lon) and supplementary details, such as vehicle speed and movement direction. Additionally, each trip is characterized by information identifying the machine, the driver and the task performed (e.g., "Transportation of rock from tunneling").

The GPS data are recorded at varying time intervals determined by the truck velocity, which results in an approximately uniform spatial resolution. The statistics of the data are presented in Table 1.

	Median	Mean and std.	Range
Timestep	2 s	$4.63 \text{ s} \pm 2.32 \text{ min}$	[0.88 s, 11.5 h]
Velocity (km/h)	8.33	9.36 ± 6.00	[0.0003, 25.93]
Distance (m)	17.13	34.97 ± 277.36	[0, 61241]
Nr points/trip	74	122.32 ± 188.90	[10, 3516]

Table 1: Data statistics: Median, mean, standard deviation (std.) and range within trips.

The data is subject to noise from several sources, including the manual nature of activity logging (such as a driver pushing a button on an iPad after loading and off-loading activities), loss or weakening of the GPS signal caused by physical obstruction (e.g., passing through tunnels), inference, or bandwidth limitations.

5. Data pre-processing

To enhance the quality of the data, the the following data pre-processing steps are performed:

1. The Haversine formula is applied to convert latitude and longitude into coordinates expressed in meters (x, y), with the origin arbitrarily set to the minimum values of latitude and longitude in the data set.
2. Incorrect or irrelevant GPS position updates are discarded, with a specific focus on the following scenarios:
 - Longitude or latitude is zero: These usually occur when the GPS device is not calibrated.
 - Velocity is zero: These are irrelevant for road inference as they do not represent movement.
 - Trip from the loading to drop-off point has fewer than N_{\min} updates: These lack the resolution necessary for precise road inference.
 - The updates occur at the conclusion of trips (trip endpoints): These are often noisy because of two reasons: a) the vehicles move slowly right before loading/unloading, which creates a challenge in refining the location by the GPS receiver¹, and b) the previous

¹GPS location is refined in the process called triangulation, which is based on the object movement.

trip is considered ongoing until the truck is being loaded again, which can result in arbitrary movement around the loading site at the end of the trip.

- Consecutive updates are duplicated: These do not improve the road inference but they increase the computational cost.

3. Each trip is interpolated with a predefined resolution ΔD_{inter} .

The hyperparameters and their default values are given in Table B.3 in the Appendix.

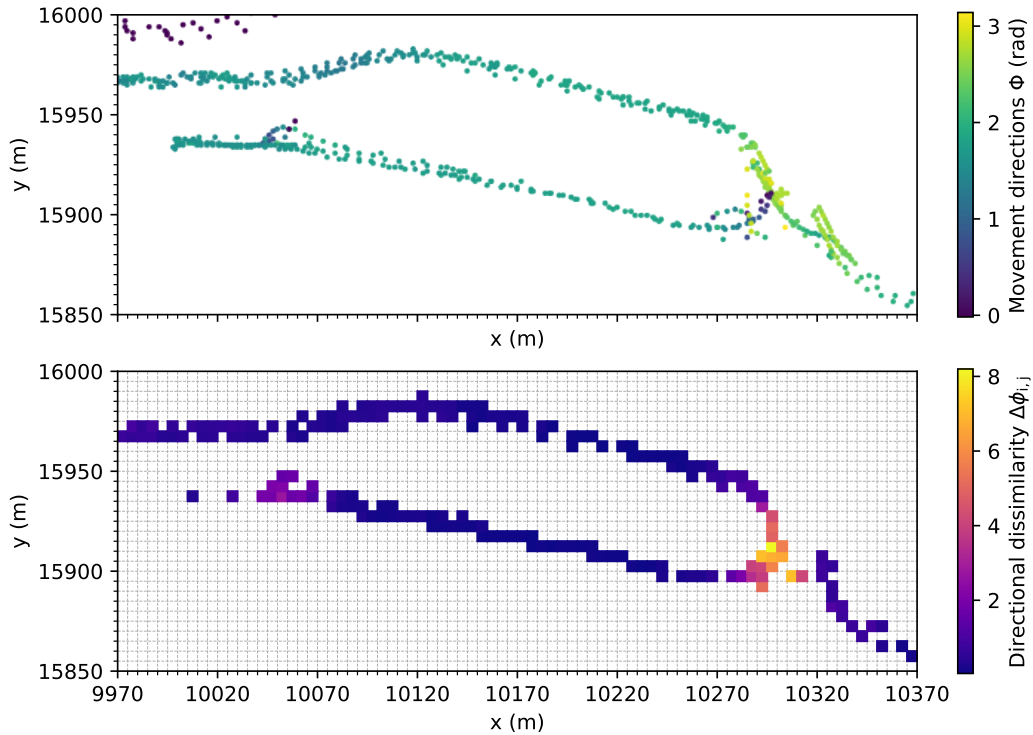


Figure 1: Identification of candidate intersections. Upper plot: The GPS trajectories are converted into movement directions $\Phi \in [0, \pi]$ (bi-directional movement, Sec. 6.1). Bottom plot: The area is split into grid cells, with the median direction determined for each cell. The median direction is then used to compute the directional dissimilarity $\Delta\phi_{i,j}$ between adjacent cells. The cells with $\Delta\phi_{i,j} \geq \Delta\phi_{\text{thr}}$ are identified as intersection candidates.

6. Graph inference algorithm

6.1. 2D histograms of heading directions

In the first step, the map is partitioned into a grid (Fig. 1). Each cell is of size $N_{\text{res}} \times N_{\text{res}} = 5 \times 5 \text{ m}^2$, and is denoted as $c_{i,j}$, where i and j are the row and column indices, respectively. The GPS trajectories, divided into trips, can then be converted into movement directions $\Phi = \{\phi_1, \phi_2, \dots, \phi_N\}$ based on the latitude and longitude of consecutive GPS updates (similar to [10]). These directions are normalized to a $[0, \pi]$ range (0 to 180°), accounting for bi-directional vehicle movement and treating travel in either direction along the same path as equivalent. Finally, for each set $\Phi_{i,j}$ of points recorded within each cell $c_{i,j}$, the median $\tilde{\phi}_{i,j}$ is computed. This procedure essentially transforms the grid into a 2D histogram, where each cell represents the median of bi-directional vehicular movement.

6.2. Identification of candidate intersections

Next, we identify potential intersection locations within the grid. These are hypothesized to be located in grid cells that have a notable deviation in vehicular movement direction relative to their adjacent cells, which is indicative of a directional change as vehicles pass through that cell.

To quantitatively identify such locations, for each cell $c_{i,j}$, we compute the directional dissimilarity $\Delta\phi_{i,j}$ defined as the root mean squared difference in the median direction between $c_{i,j}$ and its neighboring cells:

$$\Delta\phi_{i,j} = \sqrt{\sum_{k,l \in \text{neighbors}(i,j)} (\tilde{\phi}_{i,j} - \tilde{\phi}_{k,l})^2}. \quad (1)$$

Here, $\text{neighbors}(i, j)$ refers to the set of indices for cells in the neighborhood of $c_{i,j}$. A cell is considered a neighbor of $c_{i,j}$ if its center lies within a distance of $D_{\text{nbr}} = 20 \text{ m}$ or less from the center of $c_{i,j}$. Furthermore, only those cells that contain GPS data are taken into account. This approach yields higher values of $\Delta\phi_{i,j}$ for cells surrounded by numerous cells containing GPS points, which aligns with the expectation that intersections are more likely to appear in cells surrounded by many GPS tracks, rather than along well-defined straight roads, where multiple neighbors are likely to lack tracks.

A cell $c_{i,j}$ is flagged as a preliminary intersection candidate if its corresponding $\Delta\phi_{i,j}$ exceeds a predefined threshold $\Delta\phi_{\text{thr}}$. With the default cell

resolution of $N_{\text{res}} = 5$ m, this typically results in multiple adjacent cells being flagged as potential intersections. To refine these results, the neighboring candidates are further merged with a simple clustering approach. Candidates within a distance of $D_{\text{int_clust}} = 15$ m from each other are grouped together, and the central point of each group is marked as the final intersection candidate. Preliminary candidates that do not form a part of any cluster are disregarded under the assumption that the chosen N_{res} is sufficiently small for the intersections and their immediate surrounding to extend over several cells.

6.3. Validation of intersections

The next step consists of filtering out false positives among the candidate intersections using an adapted version of the method proposed in [9]. This method discerns intersections from e.g., road bends by determining the number of roads leaving the candidate location for the intersection. In our version, we first subset the GPS points to those that lie within the circle bounded by the outer radius $R + L$ and apply DBSCAN clustering. The analysis is restricted to the GPS points that are directly connected to the intersection, i.e., they form a cluster with the points passing within a distance of $D_{\text{passing}} = 15$ m. Next, following [9], we define an extremity annulus bounded by two concentric circles with radii $R = 30$ m and $R + L = 55$ m around each candidate intersection (Fig. 2). These GPS points that lie within the annulus and are connected to intersection are clustered with a clustering distance of $D_{\text{ext_clust}} = 30$ m. Each cluster with a size larger than $N_{\text{ext_clust}} = 2$ represents a road passing through the extremity. The final set of intersections are those that have at least three such clusters in their extremity, representing three roads leaving the intersection.

Depending on the actual size of intersections, this step can be repeated with varying values of R and L . To reduce computations for determining distances between the GPS points and intersections, we employed k-dimensional trees (k-d trees) that partition space into a hierarchical tree structure, significantly accelerating spatial queries. This approach allowed us to narrow down calculations only to those pairs of GPS points and intersection centers that are within a predefined maximum distance $R + L = 55$ m from each other.

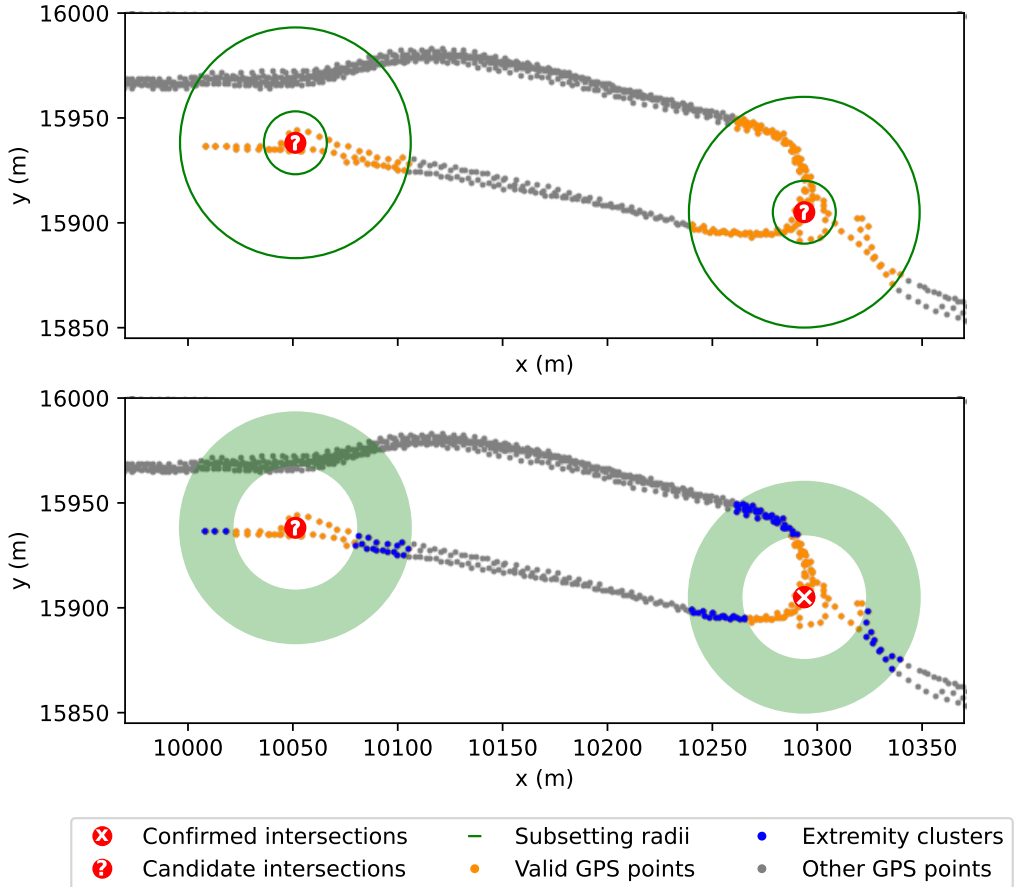


Figure 2: Validation of intersection candidates. Upper plot: the points located within the outer radius $R + L$ from each intersection candidate are clustered using DBSCAN. Those points that belong to a cluster where at least one member is within the radius D_{passing} from an intersection candidate are considered "valid points" for the next step. Bottom plot: The "valid points" are subset by annuli with radii R and $R + L$ and clustered with DBSCAN. The left candidate is rejected, as only two clusters leaving the intersection are detected, while the right candidate is accepted as it has three clusters leaving the intersection. Note that the method is robust against the presence of parallel roads that are not connected to the intersection.

6.4. Identifying load and drop-off locations

Load and drop-off locations are also considered nodes. While load and drop-off locations are reported in the data for each individual trip, due to the manual nature of the logging process they are prone to uncertainty. To minimize the uncertainty, the reported locations are clustered as follows:

- Loading points: The reported loading points are organized by the excavator ID and task ID. Within each group, the loading point is determined as the trimmed average of all positions. Loading points that are closer to each other than a predefined threshold, $D_{\text{load/dump}} = 100 \text{ m}$, are merged.
- Drop-off points: The reported drop-off points are clustered using density-based clustering (DBSCAN [12]) and the mean (lat, lon) within each cluster is used to compute the drop-off location. The locations that are closer than $D_{\text{load/dump}} = 100 \text{ m}$ are merged.

6.5. Road inference

In the final step of constructing the road network, the nodes, consisting of intersections, loading and drop-off locations, are interconnected by edges that represent the roads. Additional edges are also created to depict the roads with a dead end, i.e., the roads that pass through only one intersection.

The process starts by identifying the trip sections that pass in proximity to any node, i.e., within a predefined radius of $D_{\text{node}} = 30 \text{ m}$. For each of these sections, we mark the time step at which the GPS points are the closest to that node. The trips are then split into smaller segments at these time steps, resulting in segments that start at either the beginning of the trip or at a node, and similarly finish either at the end of the trip or at a node. The resulting segments are further grouped by their adjacent node pairs or singular nodes.

Following this, the segments in each group are assigned to clusters. The number of clusters determines the number of roads that are present in each group. The process is as follows: Firstly, all segments are trimmed around the nodes by $D_{\text{node}} = 30 \text{ m}$ (or optionally a larger distance) to avoid the separate roads connecting at these points. The GPS points within each group are clustered by their (x, y) coordinates using DBSCAN. Subsequently, each segment is assigned its dominant cluster, defined as the cluster that appears the most frequently within this segment. For each dominant cluster,

a representative segment is selected as an edge. This selection is made at random among the segments that have the median number of discretization points within the specified cluster. The final graphs consist of a list of nodes and edges that either interconnect two nodes or are connected to a node.

7. Results

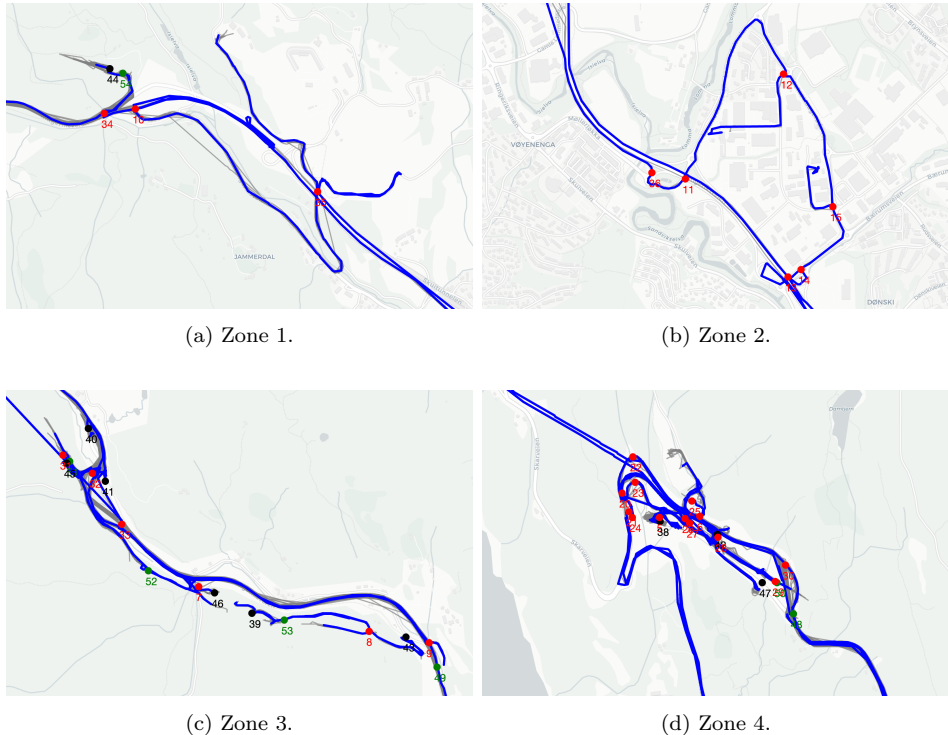


Figure 3: Examples of the inferred graph with three types of nodes representing intersections (red), load points (green), and drop-off points (black), and edges representing the roads (blue). The actual GPS data are represented by gray lines.

The visual representation of the algorithm’s performance is presented in Fig. 3. Each of the four subplots show segments of the inferred graph, in the order from relatively straightforward to more complex scenarios. The parameters used are defined in the Appendix. The intersection validation step was run twice, with $R = 30$ m and $R = 100$ m (Fig. 4).

In the first two examples: Zone 1 and 2, the algorithm achieves perfect recall and precision: All intersections are detected correctly and all driven

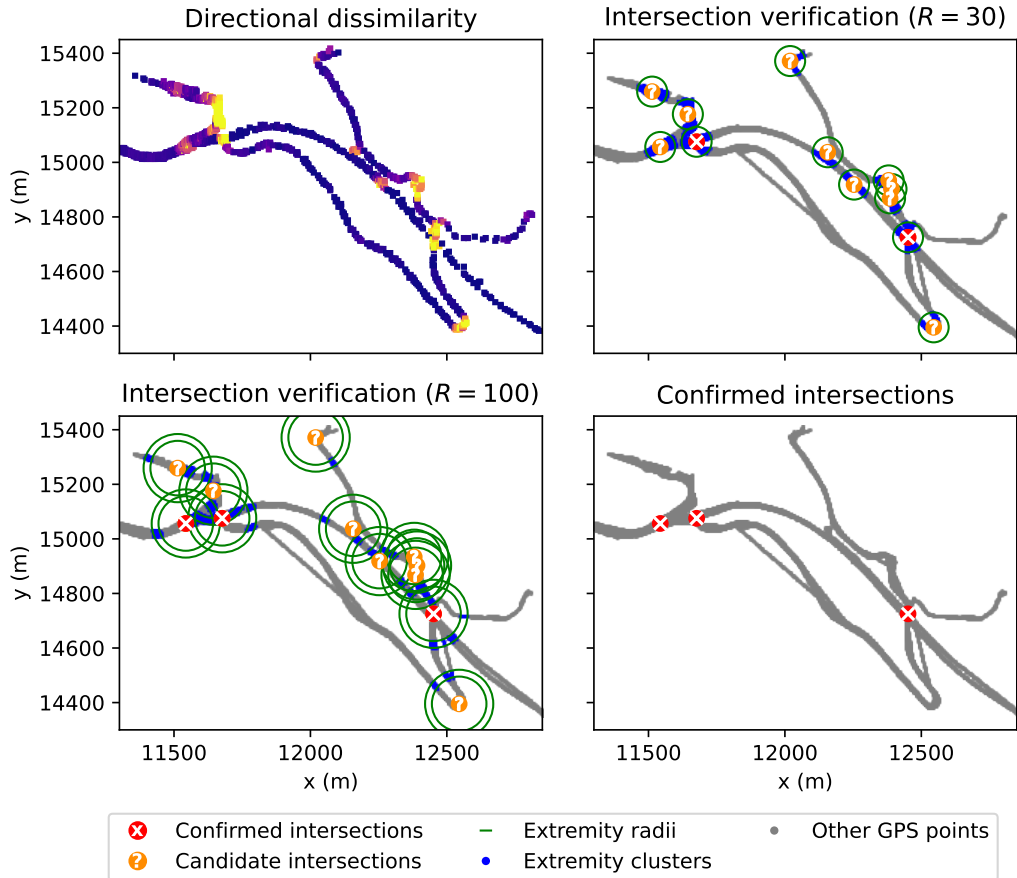


Figure 4: Step-by-step intersections detection and validation in Zone 1. Upper left: The flare-ups in directional dissimilarity suggest possible intersections. Upper right: The intersection candidates are verified with an annulus of a small radius $R = 30$. Road bends and vehicle turning points that do not have three outward roads are discarded. Bottom left: The step is repeated with a larger radius $R = 100$, allowing to find the third intersection. Bottom right: Only three intersections are confirmed, which is the correct result.

roads are outlined. The use of at least two radii in the intersection validation step is crucial to detect cross-roads of varying shape and spread, e.g., merging roads (34, Zone 1) and small detours (14, Zone 2). We note that the algorithm is robust against noisy GPS updates present in Zone 1 (visible as straight lines). This robustness against noise that visually resembles a road split is gained when quantifying the directional dissimilarity (Sec. 6.2), as the area is never qualified as an intersection candidate (see upper left in Fig. 4).

In our further analysis we show the limitation of the algorithm in the presence of consistent noise. In Zone 3 four intersections are detected correctly (7, 8, 9, and 32). Number 33 is falsely identified as an intersection due to the noisy data, while an actual merging of the roads is located 100 m to the left. In this case, the noisy updates are more frequent than the correct outline of the road. Zone 4 presents the biggest challenge to the algorithm, with noisy data dominating several parts of the map, in the areas where the vehicles often change direction. In this case, the algorithm detects several false positive intersections, e.g., number 23, or 30.

8. Discussion

While the proposed method was demonstrated to efficiently map the structure of large road networks and finding intersections, the accuracy of the method depends on two factors:

- a) Contextual parameter tuning: The algorithm's parameters have to be tuned for the specific application and characteristics of the landscape. For instance, the distance parameters that define the relevant area surrounding a singular point marked as an intersection will vary depending on the area covered by an intersection: a well-defined crossroad will need tighter parameter settings than more expansive roundabouts or open-area nodes with several diverging routes.
- b) Quality of the GPS data: While multiple problems with the data can be addressed with the steps outlined in Sec. 5, mitigating certain types of noise is not trivial, especially if the inaccurate GPS updates are dominant and overshadow valid data. Customizing the data cleansing procedure may become essential in specific deployment contexts.

9. Conclusions

Our findings highlight both the strengths and limitations of our proposed method. Notably, the algorithm demonstrates high level of proficiency in mapping large road networks and identifying road intersections and is able to achieve perfect precision and recall when the data quality is sufficient. On the other hand, the performance of our approach depends on the selection of parameters, indicating the necessity for a tailored approach rather than a one-size-fits-all solution across varied terrains. This automated graph construction approach will allow for improved coordination and management of units at construction site.

Acknowledgements

This work is based upon the support from the Research Council of Norway under project Datadrevet Anleggslass 309797 (English: Data-driven Construction Site). The data was collected by Skanska Norway AS and accessed through the Ditio app².

Author contributions

- Katarzyna Michałowska: Conceptualization, methodology development (primary), coding and implementation, visualizations, analysis, writing (original draft),
- Helga Margrete Bodahl Holmestad: Conceptualization, methodology development, coding and implementation, visualizations, writing (review and editing),
- Signe Riemer-Sørensen: Conceptualization, methodology development, writing (review and editing), resources.

Data availability

The data used in this study are proprietary to Skanska AS and can be made available upon reasonable request.

²<https://ditioapp.com/>

Conflict of interest

Authors state no conflict of interest.

References

1. Larsen HN. Bygg- og anleggssektorens klimagassutslipp. Asplan Viak by acquisition from Byggenæringens Landsforening 2019
2. Vignisdóttir HR, Kjellmark G, Kristensen T, Laanke B, Rise T, and Schmidt-Melbye PNH. Veikart for grønn anleggssektor. Norwegian. SINTEF 2021; SINTEF;2021:00552
3. Dardouri S, BuHamdan S, Balkhy WA, Dakhli Z, Danel T, and Lafhaj Z. RFID platform for construction materials management. International Journal of Construction Management 2023; 23:2509–19. DOI: 10.1080/15623599.2022.2073085. Available from: <https://doi.org/10.1080/15623599.2022.2073085>
4. Li Y and Liu C. Applications of multirotor drone technologies in construction management. International Journal of Construction Management 2019; 19:401–12. DOI: 10.1080/15623599.2018.1452101. Available from: <https://doi.org/10.1080/15623599.2018.1452101>
5. Bastani F, He S, Abbar S, Alizadeh M, Balakrishnan H, Chawla S, Madden S, and DeWitt D. RoadTracer: Automatic Extraction of Road Networks from Aerial Images. *2018 IEEE/CVF Conference on Computer Vision and Pattern Recognition*. 2018 :4720–8. DOI: 10.1109/CVPR.2018.00496
6. Mattyus G, Luo W, and Urtasun R. DeepRoadMapper: Extracting Road Topology From Aerial Images. *Proceedings of the IEEE International Conference on Computer Vision (ICCV)*. 2017 Oct
7. Costea D and Leordeanu M. Aerial image geolocalization from recognition and matching of roads and intersections. *Proceedings of the British Machine Vision Conference (BMVC)*. Ed. by Richard C. Wilson ERH and Smith WAP. BMVA Press, 2016 Sep :118.1–118.12. DOI: 10.5244/C.30.118. Available from: <https://dx.doi.org/10.5244/C.30.118>
8. He Y, Garg R, and Chowdhury AR. TD-Road: Top-down road network extraction with holistic graph construction. *Computer Vision–ECCV 2022: 17th European Conference, Tel Aviv, Israel, October 23–27, 2022, Proceedings, Part IX*. Springer. 2022 :562–77

9. Mariescu-Istodor R and Fränti P. CellNet: Inferring Road Networks from GPS Trajectories. *ACM Trans. Spatial Algorithms Syst.* 2018 Sep; 4. doi: 10.1145/3234692. Available from: <https://doi.org/10.1145/3234692>
10. Xie X, Bing-YungWong K, Aghajan H, Veelaert P, and Philips W. Inferring Directed Road Networks from GPS Traces by Track Alignment. *ISPRS International Journal of Geo-Information* 2015; 4:2446–71. doi: 10.3390/ijgi4042446. Available from: <https://www.mdpi.com/2220-9964/4/4/2446>
11. Prabowo A, Koniusz P, Shao W, and Salim FD. COLTRANE. *Proceedings of the 6th ACM International Conference on Systems for Energy-Efficient Buildings, Cities, and Transportation*. ACM, 2019 Nov. doi: 10.1145/3360322.3360853. Available from: <https://doi.org/10.1145/3360322.3360853>
12. Schubert E, Sander J, Ester M, Kriegel HP, and Xu X. DBSCAN Revisited, Revisited: Why and How You Should (Still) Use DBSCAN. *ACM Trans. Database Syst.* 2017 Jul; 42. doi: 10.1145/3068335. Available from: <https://doi.org/10.1145/3068335>

Appendix A. Nomenclature

Notion	Explanation
GPS	Global positioning system.
Intersection	A point in space where at least three roads meet.
Trip	A series of consecutive GPS points from loading a truck until a new trip starts (the truck is re-loaded).
(lat, lon)	Coordinates expressed as latitude and longitude.
(x, y)	Coordinates expressed in meters with the origin set to the minimal values of latitude and longitude in the dataset.
DTW	Dynamic time warping.

Table A.2: Nomenclature used in the paper.

Appendix B. Algorithm and data processing parameters

Symbol	Description	Default
Pre-processing parameters		
$D_{\text{endpoints}}$	Distance driven removed at the end of each trip.	100 m
d_{spline}	Spline degree used for interpolation.	1
ΔD_{interp}	Resolution applied during interpolation.	10 m
N_{min}	Minimum number of data points required to define a trip.	4
Δt_{gap}	Time threshold (in minutes) for splitting a trip into two separate trips if the vehicle is idle.	5 min
$\Delta\phi_{\text{gap}}$	Angular threshold for splitting a trip into two separate trips based on directional changes.	180°
Intersection parameters		
N_{res}	Resolution of grid cells (height and width).	5 m
D_{nbr}	Maximum distance between the centers of grid cells to consider them neighboring.	20 m
$\Delta\phi_{\text{thr}}$	Threshold for angle variation within neighboring cells to identify intersection candidates.	1.4°
$D_{\text{int_clust}}$	Clustering distance for merging intersection candidates.	15 m
L	Width of extremity annulus used for clustering.	25 m
R	Inner radius of extremity annulus used for clustering.	30 m
D_{passing}	Maximum distance allowed between the trip and the intersection center to include the GPS points belonging to that trip when validating an intersection.	15 m
$D_{\text{ext_clust}}$	Clustering distance for points in extremity annulus.	30 m
$N_{\text{ext_clust}}$	Minimum number of points in a cluster.	5
Loading and drop-off nodes parameters		
$\epsilon_{\text{load/dump}}$	Radius for expanding clusters in DBSCAN when merging loading or drop-off locations.	0.001
$D_{\text{load/dump}}$	Distance threshold for merging loading or drop-off locations.	100 m
Edge parameters		
D_{node}	Maximum distance between GPS track and the node center to consider the trip as passing through that node.	30 m
ϵ_{road}	Radius for expanding clusters in DBSCAN in road segment detection.	12 m
$N_{\text{min_road}}$	Minimal sample count in DBSCAN to form a cluster in road segment detection.	5

Table B.3: Algorithm and data-processing parameters.